Available online at www.sciencedirect.com
SCIENCE DIRECT®
Journal of Power Sources 125 (2004) 62–69
JOURNAL OF POWER SOURCES
www.elsevier.com/locate/jpowsour

Structural design considerations for micromachined solid-oxide fuel cells

V.T. Srikar, Kevin T. Turner*, Tze Yung Andrew Ie, S. Mark Spearing

Department of Aeronautics and Astronautics, Massachusetts Institute of Technology, Building 41-317, 77 Massachusetts Avenue, Cambridge, MA 02139, USA

Received 30 June 2003; accepted 24 July 2003

Abstract

Micromachined solid-oxide fuel cells (μSOFCs) are among a class of devices being investigated for portable power generation. Optimization of the performance and reliability of such devices requires robust, scale-dependent, design methodologies. In this first analysis, we consider the structural design of planar, electrolyte-supported, μSOFCs from the viewpoints of electrochemical performance, mechanical stability and reliability, and thermal behavior. The effect of electrolyte thickness on fuel cell performance is evaluated using a simple analytical model. Design diagrams that account explicitly for thermal and intrinsic residual stresses are presented to identify geometries that are resistant to fracture and buckling. Analysis of energy loss due to in-plane heat conduction highlights the importance of efficient thermal isolation in microscale fuel cell design.
© 2003 Elsevier B.V. All rights reserved.

Keywords: Portable power generation; Solid-oxide fuel cell; MEMS

1. Introduction

There is growing interest in the application of microscale devices (also called microelectromechanical systems, MEMS) for portable power generation [1–11]. It is envisioned that devices with overall dimensions on the order of millimeters, and containing components with critical dimensions in the range 0.1–10 μm, will provide between 0.5 and 50 W of power to enable the operation of other microsystems (such as sensors and actuators) and portable electronic devices (such as radios and cell phones). The device concepts being investigated include miniaturized gas-turbine engines [4], micro batteries [5], proton exchange membrane fuel cells [6–9], and solid-oxide fuel cells (SOFCs) [9–11]. The last mentioned is the focus of this paper.

The principle of operation of solid-oxide fuel cells is well known [12,13]. The active electrochemical element is a three-layer composite structure consisting of two electrodes separated by a solid-oxide electrolyte. The essential fuel cell reaction is the combination of hydrogen and oxygen to form water. The electrons participating in this reaction flow from the anode to the cathode through an external circuit, generating direct electric current in the process, and the electrical circuit is completed by the flow of oxygen ions from the cathode to the anode through the solid-oxide electrolyte. Such structures can be realized in both planar and tubular geometries [13].

The fabrication and performance of planar solid-oxide fuel cells containing thick-film (>10 μm) layers, derived from powder- and solution-processing routes, has received considerable attention [13]. Since the ionic resistance of the electrolyte scales with the thickness, it is believed that reducing the component thickness can lead to improved performance. This belief has motivated recent efforts, using a combination of vapor-phase thin film deposition and silicon micromachining techniques, to manufacture microscale solid-oxide fuel cells (μSOFCs) [9–11]. Indeed, Jankowski et al. [9] have measured the performance of a μSOFC containing a 1.2-μm thick yttria-stabilized zirconia (YSZ) electrolyte, 0.5-μm thick nickel anode, and 0.8-μm thick silver anode; this composite membrane was supported on a 0.5-mm thick, micromachined, single-crystal silicon platform (Fig. 1).

Optimization of the performance and reliability of microscale solid-oxide fuel cells requires the development of robust, *scale-dependent*, design methodologies. The ultimate goal is to identify combinations of materials, structural geometries, and processing routes that will optimize the electrochemical performance, minimize thermal losses, and ensure structural stability and reliability. The primary challenges, from the viewpoint of structural design, are enumerated below.

* Corresponding author. Tel.: +1-617-253-7214.
E-mail address: kturner@mit.edu (K.T. Turner).

0378-7753/$ – see front matter © 2003 Elsevier B.V. All rights reserved.
doi:10.1016/j.jpowsour.2003.07.002

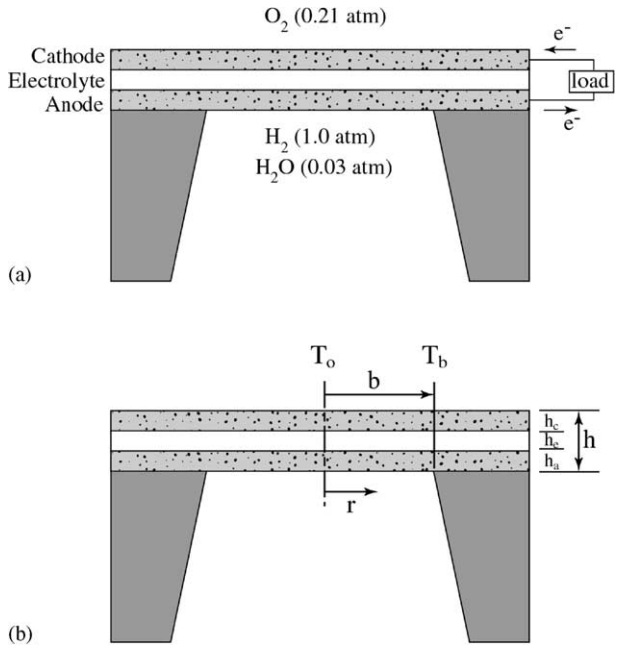

Fig. 1. (a) Schematic side-view of a three-layer solid-oxide fuel cell consisting of porous electrodes and dense electrolyte. (b) Critical dimensions and operating temperatures. The in-plane dimension, b, is ∼mm, while the thickness, h, is ∼μm.

(i) The benefits offered, and constraints imposed, by microfabrication techniques are considerably different from those of conventional machining methods. In particular, micromachining permits the parallel fabrication of arrays of geometrically-complex, two-dimensional, structures, but extensions to three-dimensions are mostly limited to extrusion-type processes [14]. Planar designs of the type shown in Fig. 1 are considerably easier to realize compared to tubular structures.

(ii) Thin film materials are invariably subjected to *intrinsic* residual stresses (σ_{res}) originating from the details of the growth processes [14]. It is well established that intrinsic stresses are strong functions of the processing conditions. Moreover, systematic changes in a few processing parameters (argon gas pressure and bias voltage in sputter deposition, for instance) can lead to stress changes of several hundred megapascals in metallic and oxide thin films. This ability to *tune* the stress by controlling the process parameters implies that it is both reasonable and essential to treat σ_{res} as a design variable.

(iii) Solid-oxide fuel cells operate at temperatures of several hundred degrees centigrade. This requires that the structural stability and reliability of a three-layer composite structure be guaranteed over a wide temperature range (say, 20–650 °C). The electrode and electrolyte materials, and the supporting silicon structure, can possess significantly different thermomechanical properties, resulting in large thermal stresses (σ_{th}) during thermal excursions. Failure due to fracture (in tension) or buckling (in compression) represents a serious reliability concern.

(iv) Operation at high temperatures requires efficient thermal isolation schemes to prevent heat loss from the membrane device. The difficulty of this task increases with the degree of miniaturization since, in general, heat losses increase with decreasing device dimensions. Furthermore, it is necessary to consider coupled thermal and structural design since the structure that minimizes heat losses may not be mechanically stable.

1.1. Scope of analysis

The preceding discussion makes clear that a natural starting point for microscale solid-oxide fuel cells is the planar design of Fig. 1. In this first analysis, we present simple, analytical models to evaluate the effect of geometry on performance and reliability. Section 2 presents closed-form expressions, containing two free parameters, to estimate the cell potential and power density of a planar μSOFC. These parameters are evaluated using the experimental results of Jankowski et al. [9], and the results used to determine the effect of electrolyte thickness on fuel cell performance.

The electrodes, which are usually fabricated using silver, nickel, or nickel-YSZ cermets, are porous (or contain microfabricated through-holes) to permit gas transport to the electrode/electrolyte interfaces. The yttria-stabilized zirconia electrolyte layer is dense and relatively thick, and serves as the load-bearing structure. Therefore, as a first approximation, the structure can be modeled as a single -layer membrane with material properties corresponding to those of YSZ. Section 3 analyzes the mechanical stability and integrity of this membrane and presents a design diagram to identify geometries that are resistant to both buckling and fracture. Heat losses due to in-plane conduction, and the need for coupled design considerations, are discussed in Section 4.

2. Electrochemical performance

Consider the fuel cell structure shown in Fig. 1. The temperature of the membrane is assumed to be uniform (i.e. $T_0 = T_b$). The primary performance parameters of the fuel cell are the cell potential ($\boldsymbol{E}$) and power density (P) (i.e. the power produced *per unit membrane area*), which are related by

$$P(i) = i \cdot \boldsymbol{E}(i) \tag{1}$$

where i is the current density. In general, the cell potential can be expressed as [15]

$$\boldsymbol{E} = \boldsymbol{E}_0 - \eta_{\text{Ohmic}} - \eta_{\text{Activation}} - \eta_{\text{Concentration}}. \tag{2}$$

The open circuit voltage, $\boldsymbol{E}_0$, is dependent solely on the thermodynamics of the fuel cell reaction and has a value, given by the well known Nernst equation [13], of ∼1.0 V

for typical operating conditions under consideration. However, when current is drawn from the cell, the cell potential decreases due to several sources of polarization, η, as discussed below.

One source of polarization is due to the ohmic resistivity of the solid-oxide electrolyte to the flow of oxygen ions and is given by

$$\eta_{\text{Ohmic}} = i\frac{h_e}{\sigma_e} \tag{3}$$

where h_e and σ_e are the thickness and ionic conductivity of the electrolyte, respectively. The ionic conductivity of YSZ ranges from 0.3 to 3.0 S/m over the temperature range 600–1000 °C, respectively.

Both activation and concentration polarizations are related to the kinetics of fuel cell reactions. The first is due to the activated processes involved in charge transfer at the electrode/electrolyte interfaces and can be expressed as [15]

$$\eta_{\text{Activation}} = \frac{RT_0}{nF}\left(\frac{i}{i_1}\right) + \frac{2RT_0}{nF}\ln\left(\frac{i}{i_2}\right). \tag{4}$$

Here R is the gas constant (8.314 J/K/mol), F the Faraday constant (96485 C/mol), n the number of electrons exchanged per oxygen ion (hence, $n = 2$), and T_0 the operating temperature of the fuel cell (assumed to be uniform over the membrane). The exchange current densities i_1 and i_2 are typically treated as free parameters and obtained from fits to measurements. Each of the two terms in Eq. (4) corresponds to the limiting cases of the more general Volmer–Butler analysis of the kinetics of activated processes [18].

The concentration polarization is due to diffusion-limited processes (such as transport of fuel to the active sites on the membrane) in the operation of the fuel cell [15]. Analytical expressions for the concentration polarization of conventional fuel cells are usually complicated functions of microstructural parameters of the electrodes and electrolytes. In this first analysis, it is assumed that $\eta_{\text{Concentration}} = 0$. This is reasonable since, the smaller the dimensions of the device, the smaller the relevant diffusion lengths, and the less important any concentration-induced polarizations.

With this assumption, and combining Eqs. (1)–(4), we obtain

$$\boldsymbol{E} = \boldsymbol{E}_0 - \frac{ih_e}{\sigma_e} - \frac{RT_0}{2F}\left(\frac{i}{i_1}\right) - \frac{RT_0}{F}\ln\left(\frac{i}{i_2}\right), \tag{5}$$

$$P = i\boldsymbol{E} = i\left[\boldsymbol{E}_0 - \frac{ih_e}{\sigma_e} - \frac{RT_0}{2F}\left(\frac{i}{i_1}\right) - \frac{RT_0}{F}\ln\left(\frac{i}{i_2}\right)\right]. \tag{6}$$

These expressions are independent of the shape of the membrane since the temperature is assumed to be uniform.

The exchange current densities are evaluated by fitting (5) and (6) to the measurements of Jankowski et al. [9].

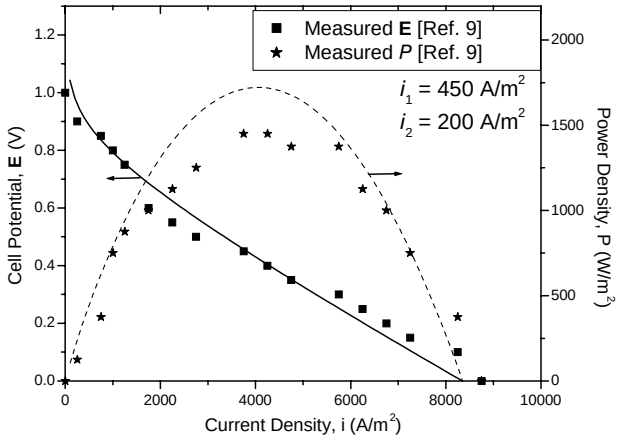

Fig. 2. Electrochemical performance of microscale solid-oxide fuel cell. The data correspond to the measurements of Jankowski et al. [9]. The curves correspond to an analytical model that treats the exchange current densities as fitting parameters.

Fig. 2 shows that values of 200 and 450 A/m^2 result in good agreement with the data obtained at 600 °C. These values are comparable to the exchange current densities reported in thick-film SOFCs at similar temperatures [19]. Values for exchange current densities at 490 and 550 °C were obtained by similar analysis (Table 1). This table shows that the average power density in μSOFCs is ∼10^3 W/m^2 at the temperatures indicated. Hence, a power output of 1 W requires a circular membrane of radius ∼2 cm.

Eqs. (5) and (6) can be used to evaluate the effect of electrolyte thickness on performance. Fig. 3 indicates that, even for membranes as thick as 2 μm, the activation polarization dominates over ohmic losses at the temperatures considered, and a further reduction in thickness is not expected to result in improved power density. Therefore, the choice of membrane thickness can be guided primarily by mechanical and thermal considerations as explained in the following sections.

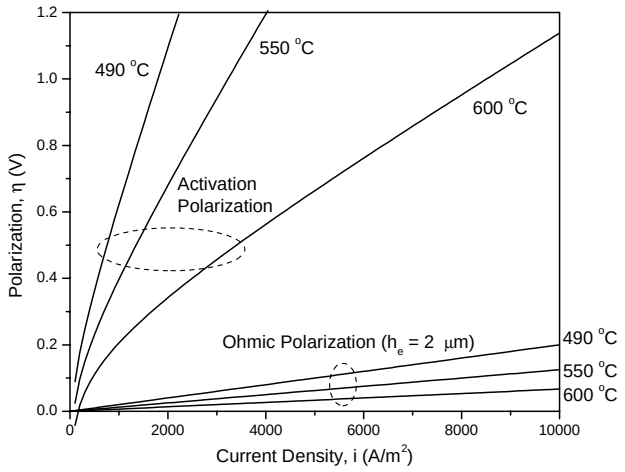

Fig. 3. Comparison of activation and ohmic polarizations for a microscale solid-oxide fuel cell.

Table 1
Measured and fitted μSOFC parameters

	Temperature, T_0		
	763 K (490 °C)	823 K (550 °C)	873 K (600 °C)
Ionic conductivity of YSZ, σ_e (S/m) [17]	0.1	0.16	0.3
Peak power density, P (W/m^2) [9]	360	730	1450
RT_0/F	0.065	0.071	0.075
Exchange current density, i_1 (A/m^2)	75	150	450
Exchange current density, i_2 (A/m^2)	50	100	200

3. Structural reliability and stability

The composite membrane shown in Fig. 1 is invariably subjected to intrinsic (σ_{res}) and thermal (σ_{th}) residual stresses. It is well known that layered structures are susceptible to stress-induced failure by several modes including fracture, buckling, interlaminar delamination, and spalling [20]. Examining all these modes in a composite membrane complicates the design process significantly. As mentioned previously, however, we consider here a class of structures in which two layers are porous and the third (electrolyte) is relatively thick, dense, brittle, and serves as the primary load-bearing structure. Hence, for first-order design, the design of this single membrane, assumed to be circular with radius b and thickness h, against fracture and buckling is investigated. The material is assumed to be isotropic and homogeneous, and has a Young's modulus E, Poisson's ratio ν, and coefficient of thermal expansion α. (The thermal expansion coefficient of the supporting structure is α_s; Table 2.) As before, it is assumed that $T_0 = T_b$.

Since the membrane is supported by a relatively large and stiff silicon structure, it is reasonable to assume clamped boundary conditions. The validity of this assumption was verified using finite-element computations. Similarly, since the gaseous streams on either side of the membrane are at approximately equal pressures, we assume that there is no pressure differential across the membrane. The thermal stress, which can be readily obtained by integrating the thermal strain over the diameter of the membrane and subsequently employing Hooke's law, is given by [21]

$$\sigma_{th} = \frac{-E}{1-\nu}(\alpha - \alpha_s)(T_0 - T_{RT}) = \frac{-E}{1-\nu}\Delta\alpha\,\Delta T, \tag{7}$$

where T_{RT} is room temperature. A positive ΔT, which corresponds to expansion of an unclamped membrane, induces compressive thermal stresses in the clamped membrane ($\sigma_{th} < 0$), as expected.

Table 2
Nominal material properties at 300 K [16]

	Yttria-stabilized zirconia (YSZ)	Silicon
Young's modulus, E	200 GPa	160 GPa
Poisson ratio, ν	0.2	0.2
Coefficient of thermal expansion, α	10×10^{-6} K^{-1}	3×10^{-6} K^{-1}
Density, ρ	6000 kg/m^3	2320 kg/m^3

Estimation of intrinsic residual stresses is non-trivial and usually requires experimentation, especially for the complex oxide materials of interest in fuel cells. Previous measurements suggest that it is possible to tune the intrinsic stress in YSZ thin films over a large range by suitable choice of processing technique (sputtering and electron-beam evaporation, for instance) and processing parameters [11,22–24]. It is assumed here that σ_{res} is independent of temperature, although this is strictly true only if the film microstructure remains invariant during thermal excursion.

3.1. Stress-induced failures

The total stress (σ) in the membrane is the sum of the thermal and intrinsic components and can be expressed as

$$\sigma = \sigma_{res} + \sigma_{th} = \sigma_{res} - \frac{E}{1-\nu}\Delta\alpha\,\Delta T. \tag{8}$$

If the stress in the membrane is sufficiently compressive, then failure will occur via buckling. For a circular plate that is clamped at the edges, the critical stress at which buckling occurs is given by [25,26],

$$\sigma_{cr} = -1.22\frac{E}{1-\nu^2}\left(\frac{h}{b}\right)^2. \tag{9}$$

Thus, large area, thin membranes (i.e. small (h/b)), which are desirable from the viewpoint of electrochemical performance, are seen to be particularly susceptible to buckling.

The primary mode of failure in tension is brittle fracture due to the nucleation and growth of cracks [27]. The simplest criterion assumes that fracture occurs when

$$\sigma \geq \sigma_f \tag{10}$$

where σ_f is the fracture strength of the structure. However, the fracture strength of brittle materials (such as yttria-stabilized zirconia) is a distributed quantity and probabilistic methods are required for reliable design. In the widely used Weibull method, such design is accomplished by first fitting experimentally measured fracture strengths of nominally identical specimens (of volume V_0) to a two-parameter Weibull function [27]. These parameters are the reference strength, σ_0, which is the stress at which 63% of the specimens fail, and a Weibull modulus, m, which is a measure of

the degree of scatter in the fracture strength. The probability of failure of a structure of volume V can be expressed as

$$P_f = 1 - \exp\left(-\frac{V}{V_0}\left[\left(\frac{\sigma_1}{\sigma_0}\right)^m + \left(\frac{\sigma_2}{\sigma_0}\right)^m + \left(\frac{\sigma_3}{\sigma_0}\right)^m\right]\right) \quad (11)$$

where σ_1, σ_2, and σ_3 are the principal stresses in the structure. The stress state in the membranes can be approximated to be equibiaxial such that $\sigma_1 = \sigma_2 = \sigma$ and $\sigma_3 = 0$. For the purpose of design, it is convenient to specify a tolerable probability of failure, and compute the maximum stress that can be imposed on the structure. Using the geometry defined in Fig. 1, and using Eq. (11), the maximum stress can be expressed in terms of the Weibull parameters as

$$\sigma \geq \sigma_0\left[-\frac{1}{2}\frac{V_0}{\pi b^2 h}\ln(1 - P_f)\right]^{1/m}. \quad (12)$$

The Weibull parameters for vapor-deposited YSZ thin films are currently unknown.

3.2. Design diagram

Eqs. (8), (9), and (12) can be used to construct a design diagram (Fig. 4), with axes corresponding to the intrinsic residual stress and the imposed temperature change. This map shows the effects of these parameters on the total stress in the membrane. The stresses are compressive above, and tensile below, the reference line corresponding to $\sigma = 0$. The stress limits for buckling and fracture are shown on the map. A further limitation is placed by the practical consideration that $\Delta T > 0$ (i.e. the membrane is typically never cooled below room temperature either during fabrication or operation) and that the membrane be stable at $\Delta T = 0$. Using these limits, a safe design space can be highlighted on the map. Clearly, the maximum permissible temperature excursion can be increased by increasing the membrane aspect ratio (h/b). The same goal can also be achieved by decreasing $\Delta\alpha$, although the limited choice of electrochemically active materials, and substrates for microfabrication, is expected to restrict this option.

With this approximation, and for membranes with negligible intrinsic residual stress, Fig. 5 shows a plot of the maximum permissible temperature excursion as functions of membrane geometry. For a 1-μm thick membrane operating at 600 °C, this graph suggests a maximum in-plane radius of only 17 μm. This in itself does not represent a serious limitation since large arrays of small, circular, membranes can be processed in parallel to obtain the requisite large (∼cm^2) active areas.

Alternately, the mechanical stability of the membrane can be increased either by choosing other shapes or by using stiffening structures. Fig. 6 shows the computed critical buckling stresses for clamped, equal-area, membranes of different shapes and indicates that rectangles have modestly higher resistance to buckling compared to squares

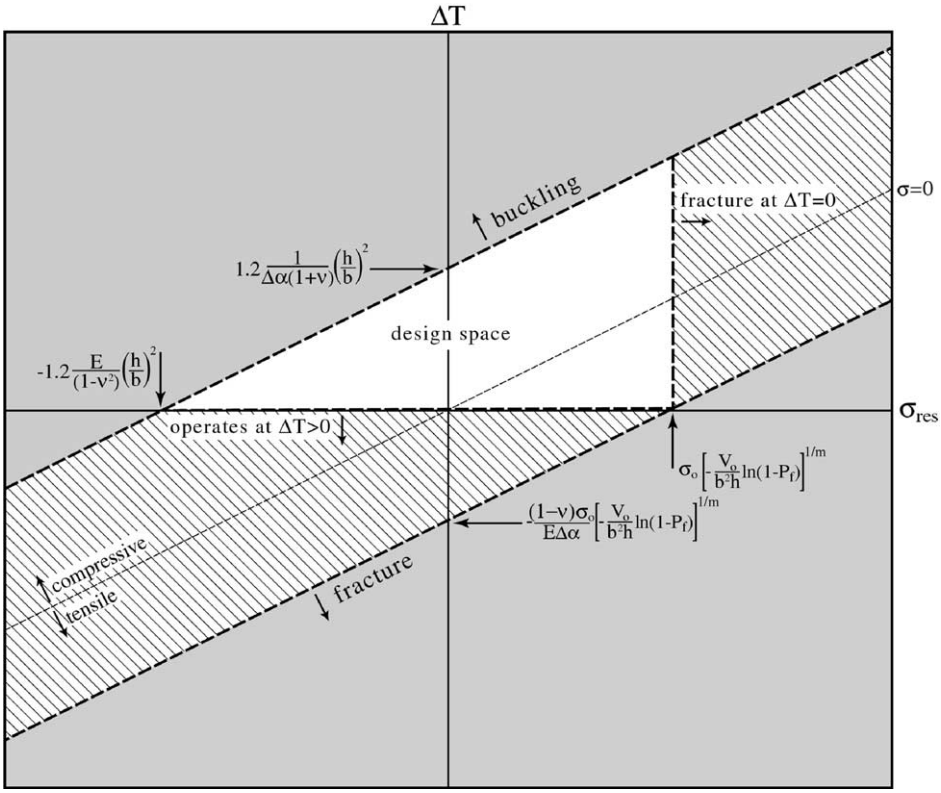

Fig. 4. Design map to select membrane geometries resistant to buckling and fracture. The maximum permissible temperature change, ΔT, is plotted as a function of the intrinsic residual stress, σ_{res}. The central triangular region contains membrane geometries resistant to both fracture and buckling.

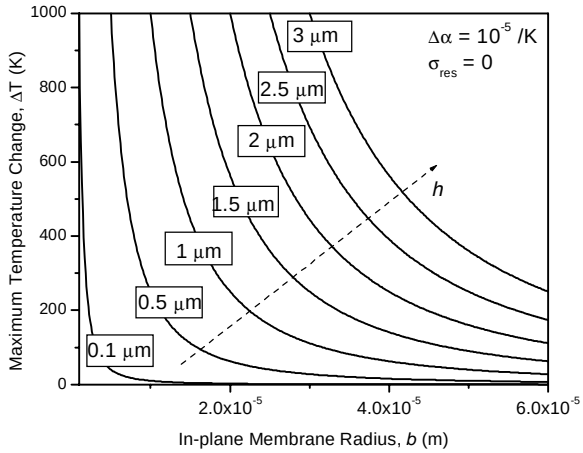

Fig. 5. Maximum permissible temperature change for yttria-stabilized zirconia membranes as functions of radius and thickness. The intrinsic stress is assumed to be zero.

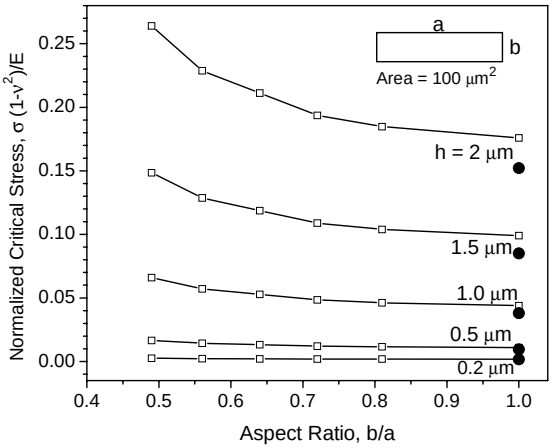

Fig. 6. Normalized critical buckling stress for equal-area rectangular membranes as functions of the aspect ratio of side lengths. The circles indicate the corresponding stress values for circular membranes of the same area.

and circles. A more promising strategy is to pattern silicon nitride stiffeners as supports for the zirconia film, as illustrated in Fig. 7. Preliminary finite-element calculations indicate that the effect of such stiffeners is to impose clamped boundary conditions on each sub-unit of the electrolyte membrane, thereby increasing the resistance to buckling. Detailed numerical analysis of the mechanical behavior of stiffened membranes is an area of our current research.

4. Thermal performance

Thermal losses may occur during the operation of fuel cells through convection to the working fluids, radiation to the surroundings, and conduction in the structure. Conductive losses are considered here since they directly influence the structural design of the device. In contrast to the assumption of uniform operating temperature of the previous sections, we now consider the membrane to be subjected to an in-plane gradient such that the temperature is T_0 at the center, and $T_b = T_{RT}$ at the boundaries. Practically, such a profile may be maintained by distributing thin-film heaters on the membrane and cooling the substrate.

Under the assumption of uniform heating, the temperature distribution in the membrane as a function of radial position, r, is parabolic [28],

$$T(r) = T_0 - (T_0 - T_b)\left(\frac{r}{b}\right)^2. \tag{13}$$

The power per unit membrane area, Q, required to maintain this temperature profile is

$$Q = k\left(\frac{h}{b^2}\right)(T_0 - T_b) = k\left(\frac{h}{b^2}\right)\Delta T, \tag{14}$$

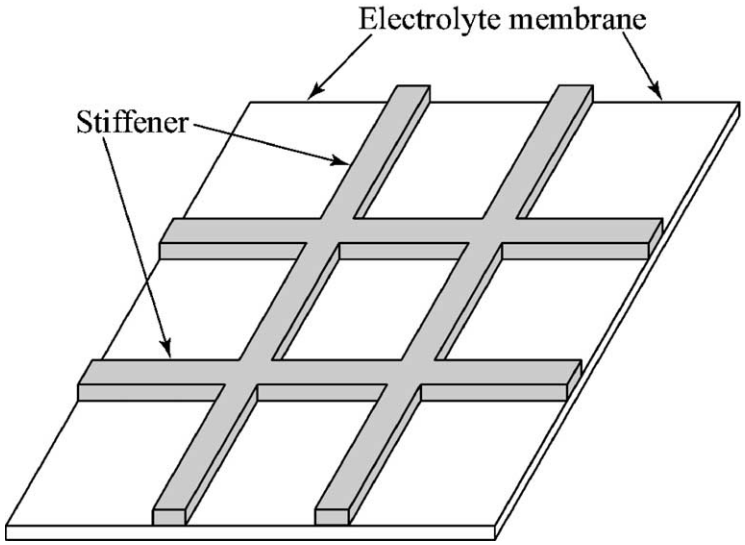

Fig. 7. Schematic of patterned stiffeners that may be used to prevent buckling of thin-film fuel cell membranes. Stiffeners offer the possibility to increase the buckling load without significantly increasing the thermal conduction losses from the membrane.

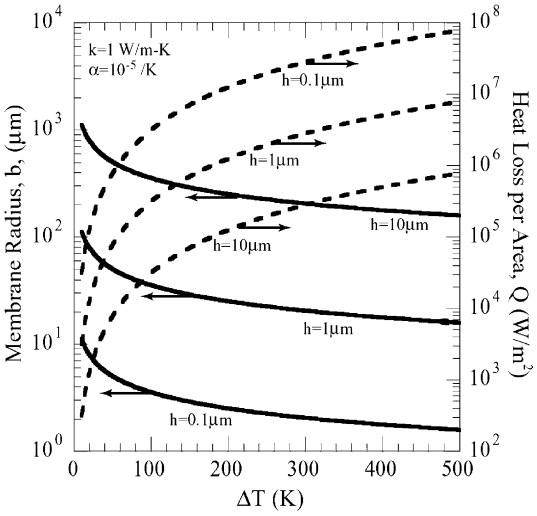

Fig. 8. Heat loss per unit membrane area and membrane radius design curves. Heat loss increases with decreasing thickness because thinner membranes require a smaller diameter to resist buckling.

where k is the thermal conductivity of the membrane. The thermal analysis can now be coupled with the preceding structural considerations by combining Eqs. (7)–(9). Assuming zero intrinsic stress, we obtain

$$Q = 3.28(1-\nu)\frac{\Delta T^2}{h}k\,\Delta\alpha \tag{15}$$

Eq. (15) represents the thermal power density required to maintain a membrane, *which is required to be resistant to buckling*, at temperatures T_0 and T_{RT} at the center and periphery, respectively. This analysis can conveniently be presented in graphical form, with separate vertical axes corresponding to the critical membrane radius, b, and Q, plotted against the temperature change, ΔT. Contrary to intuition, Fig. 8 indicates that the heat losses *increase* as the membrane is made thinner. This can be understood on the basis that, although making the membrane thinner reduces conduction heat losses, it also requires a corresponding decrease in the membrane radius to maintain structural stability. In other words, this coupled analysis captures a scaling behavior that cannot be obtained by examining the thermal performance or the structural behavior in isolation.

For a given area, a circular shape has the smallest perimeter and hence the lowest conduction heat loss. Even for this optimal shape, it is striking to note that heat loss densities are considerably larger than the generated power density for temperature gradients as small as tens of degree centigrade. Developing efficient thermal isolation schemes for μSOFCs is therefore critical for ensuring efficient fuel cell operation.

5. Summary

Microscale solid-oxide fuel cells are among a class of devices being investigated for portable power generation. As a step toward developing systematic, scale-dependent, design methodologies for such devices, we presented analytical models for the electrochemical performance, structural reliability and thermal losses for a planar, circular, electrolyte-supported, device. The principal assumptions and results are enumerated below.

(i) Expressions for the cell potential and power density were presented based on the assumption that concentration polarizations are negligible in microscale fuel cells. Values for the exchange current densities were obtained by fitting these expressions to previously measured fuel cell performance. These results were then used to evaluate the relative importance of ohmic and activation polarizations. Our results indicate that fuel cell performance is insensitive to electrolyte thickness in the micrometer range at the temperatures considered.

(ii) Layered composite thin-film structures are invariably subjected to intrinsic and thermal residual stresses. Failure due to fracture and buckling are hence serious reliability concerns. Design diagrams were presented to identify geometries that are stable and reliable.

(iii) The thermal performance of planar microscale fuel cells was analyzed assuming in-plane heat conduction to be the dominant loss mechanism. This analysis, coupled with structural considerations, enables the identification of geometries that simultaneously minimize thermal losses and ensure sufficient structural stability. However, over the range of parameters considered, thermal losses are significantly higher than the electrochemical power produced. Developing schemes for thermal isolation of microscale fuel cell devices is therefore an important area of research in this field.

Acknowledgements

This work benefited from stimulating discussions with our MIT colleagues, especially Josh Hertz, Jurgen Fleig, Chelsey Baertsch, Steve Weiss, Harry Tuller and Klavs Jensen. Financial support was provided by the DoD Multidisciplinary University Research Initiative (MURI) administered by the Army Research Office under Grant DAAD 19-01-1-05 66 U.S.

References

[1] P.B. Koeneman, I.J. Busch-Vishniac, K.L. Wood, Feasibility of micro power supplies for MEMS, J. Microelectromech. Syst. 6 (1997) 355–362.
[2] C.K. Dyer, Fuel cells for portable applications, J. Power Sources 106 (2002) 31–34.
[3] H.L. Maynard, J.P. Meyers, Miniature fuel cells for portable power: design considerations and challenges, J. Vac. Sci. Technol. B20 (2002) 1287–1297.
[4] A.H. Epstein, S.D. Senturia, Macro power from micro machinery, Science 276 (1997) 1211.

[5] J.N. Harb, R.M. LaFollette, R.H. Selfridge, L.L. Howell, Microbatteries for self-sustained hybrid micropower supplies, J. Power Sources 104 (2002) 46–51.
[6] J.P. Meyers, H.L. Maynard, Design considerations for miniaturized PEM fuel cells, J. Power Sources 109 (2002) 76–88.
[7] J.D. Morse, A.F. Jankowski, R.T. Graff, J.P. Hayes, Novel proton exchange membrane for thin-film fuel cell for microscale energy conversion, J. Vac. Sci. Technol. A 18 (2000) 2003–2005.
[8] G. D'Arrigo, C. Spinella, G. Arena, S. Lorenti, Fabrication of miniaturized Si-based electrocatalytic membranes, Mater. Sci. Eng. C 23 (2003) 13–18.
[9] A.F. Jankowski, J.P. Hayes, R.T. Graff, J.D. Morse, in: R.B. Schwarz, G. Ceder, S.A. Ringel (Eds.), Microfabricated thin-film fuel cells for portable power requirements, Proc. Mater. Res. Soc. Symp. 730 (2002) 93–98.
[10] J.L. Hertz, J. Lappaleinen, H. Tuller, Progress towards an all-thin film solid-oxide fuel cell, Proc. Electrochem. Soc. (2003), in press.
[11] C.D. Baertsch, K.F. Jensen, M.A. Schmidt, J. Hertz, H.L. Tuller, V.T. Srikar, S.M. Spearing, Fabrication and structural characterization of self-supporting electrolyte membranes for a micro solid oxide fuel cell, 2003, in preparation.
[12] N.Q. Minh, Ceramic fuel cells, J. Am. Ceram. Soc. 76 (1993) 563–588.
[13] G. Hoogers, Fuel Cell Technology Handbook, CRC Press, Boca Raton, FL, 2002.
[14] M. Madou, Fundamentals of Microfabrication, CRC Press, Boca Raton, FL, 2002.
[15] S.H. Chan, K.A. Khor, Z.T. Xia, A complete polarization model of a solid-oxide fuel cell and its sensitivity to the change of cell component thickness, J. Power Sources 93 (2001) 130–140.
[16] M.F. Ashby, Materials Selection in Mechanical Design, Butterworth-Heinemann, 1999.
[17] B.C.H. Steele, A. Heinzel, Materials for fuel-cell technologies, Nature 414 (2001) 345–352.
[18] G.W. Castellan, Physical Chemistry, Benjamin/Cummings Publishing Company, 1983.
[19] J.-W. Kim, A.V. Virkar, K.-Z. Fung, K. Mehta, S.C. Singhal, Polarization effects in intermediate temperature, anode-supported solid-oxide fuel cells, J. Electrochem. Soc. 146 (1999) 69–78.
[20] S.M. Spearing, Design diagrams for reliable layered material, AIAA J. 35 (10) (1997) 1638–1644.
[21] W.C. Young, Roark's Formulas for Stress and Strain, McGraw-Hill, New York, 1989.
[22] L.S. Wang, E.S. Thiele, S.A. Barnett, Sputter deposition of yttria-stabilized zirconia and silver cermet electrodes for SOFC applications, Solid State Ionics 52 (1992) 261–267.
[23] A.S. Kao, Comparison of zirconia thin films sputtered from metal and compound targets by reactive ion-beam process, J. Appl. Phys. 69 (1991) 3309–3315.
[24] R.W. Knoll, E.R. Bradley, Correlation between the stress and microstructure in bias-sputtered ZrO_2–Y_2O_3 films, Thin Solid Films 117 (11984) 201–210.
[25] A.C. Ugural, Stresses in Plates and Shells, McGraw-Hill, New York, 1999.
[26] S. Timoshenko, S. Woinowsky-Krieger, Theory of Plates and Shells, 2nd ed., McGraw-Hill, New York, 1959.
[27] B. Lawn, Fracture of Brittle Materials, Cambridge University Press, Cambridge, 1998.
[28] F.P. Incropera, D.P. DeWitt, Fundamentals of Heat and Mass Transfer, Wiley, London, 1996.